https://doi.org/10.5194/egusphere-2023-1393
Preprint. Discussion started: 24 October 2023

Impact of upper-level circulation on upper troposphere and lower stratosphere ozone distribution over Northeast Asia

Zhiheng Liao[a, b], Jinqiang Zhang[c, d], Yubin Pan[a, b], Xingcan Jia[a, b], Pengkun Ma[a, b], Qianqian Wang[a, b], Zhigang Cheng[a, b], Lindong Dai[a, b], Jiannong Quan[a, b]

[a] Institute of Urban Meteorology, Chinese Meteorological Administration, Beijing, China

[b] Key Laboratory of Urban Meteorology, China Meteorological Administration, Beijing, China

[c] Key Laboratory of Middle Atmosphere and Global Environment Observation, Institute of Atmospheric Physics, Chinese Academy of Sciences, Beijing, China

[d] College of Earth and Planetary Sciences, University of Chinese Academy of Sciences, Beijing 100049, China

Corresponding author: Z.H. Liao (lzhiheng118@163.com); J. N. Quan (jnquan@ium.cn)

Abstract: Ozone (O_3) in the upper troposphere and lower stratosphere (UTLS) is strongly regulated by upper-level circulation dynamics. Understanding the coupling between UTLS O_3 distribution and upper-level circulation dynamics is important not only to understand synoptic processes governing O_3 distribution and variability, but also to test the fidelity of chemistry transport models in simulating the stratosphere–troposphere exchange (STE) processes. This study presents the first systematic assessment of observationally constrained UTLS O_3 variability associated with upper-level circulation patterns over the Northeast Asia region. By applying the self-organized mapping (SOM) technique to 500, 250, and 100 hPa geopotential height (GPH) data, 12 circulation patterns are quantified and then used to characterize the UTLS O_3 distribution in the period 2000–2020 in both four-site (Beijing, Pohang, Tateno, and Sapporo) ozonesonde data and regional-scale satellite products. The underlying dynamic transport mechanism responsible for UTLS O_3 responses to different circulation patterns are further explored through correlation analysis between O_3 anomalies and transport indicators. The results indicate that although O_3 at almost all altitudes shows statistically significant sensitivity to circulation patterns, lower-stratospheric O_3 exhibits a far stronger sensitivity when compared with upper-tropospheric O_3. Circulation patterns featuring the East Asian Trough (EAT) show clear enhancement of O_3 southwest of the trough, and the enhancement zone moves with the eastward propagation of the EAT. Circulation patterns featuring eastward-shedding vortices of the Asia Summer Monsoon Anticyclone (ASMA) show the opposite signal, in which O_3 concentrations are decreased, especially at Sapporo, and the negative O_3 anomaly zone stretches from South Japan to Sakhalin Island. Each circulation pattern is characterized by distinct transport pathways, which play a determining role in the pattern-specific UTLS O_3 response. Positive O_3 anomalies are usually associated with post-trough downward and southward transport, whereas negative O_3 anomalies are commonly associated with fore-trough upward and northward transport. In the lower stratosphere, the correlation between O_3 anomalies and transport indicators is significantly stronger than that in the upper troposphere, and the strongest correlation occurs in the lower stratosphere of Beijing.

1 Introduction

Ozone (O_3) is one of the most important greenhouse gases in the atmosphere and plays a key role in weather and climate by modulating solar short-wave radiation and Earth long-wave radiation (Monks et al., 2015). In the upper troposphere and lower stratosphere (UTLS) region, rapidly increasing O_3 concentrations in the vertical are critical to net heating near and above the tropopause. Furthermore, per molecule O_3 radiative forcing efficiency is greatest

https://doi.org/10.5194/egusphere-2023-1393
Preprint. Discussion started: 24 October 2023

in this cold region (Lacis et al., 1990;de F. Forster and Shine, 1997;Riese et al., 2012), implying that subtle O_3 changes can lead to substantial temperature changes. The strong radiative modulation to vertical temperature gradient may influence the near-tropopause potential vorticity gradient (Chagnon et al., 2013;Attinger et al., 2019), which acts as a waveguide for Rossby waves (Martius et al., 2010;Grams et al., 2011) and eventually affects downstream weather development at mid-latitudes (Petzoldt et al., 1994;Peters et al., 2015). Therefore, understanding the sources and controls of UTLS ozone variability is essential to better understand weather and climate system. Specifically, it is vital to understand processes that facilitate air exchange across the tropopause (stratosphere–troposphere exchange; STE), as this can significantly and rapidly alter the composition and radiative forcing in the UTLS region.

Climatically, O_3 abundances in the stratosphere are more than an order of magnitude greater than those in the troposphere. The vertical distribution of UTLS O_3 is thus strongly modulated by the STE processes, including two directions referred to as stratosphere-to-troposphere transport (STT) and troposphere-to-stratosphere transport (TST) (Holton et al., 1995;Olsen et al., 2004). Globally, the STE is unbalanced, with net STT in the extratropics and net TST in the tropics. Such imbalance is mainly attributed to Brewer–Dobson circulation, a latitudinal circulation characterized by tropospheric air rising into the tropical lower stratosphere, moving poleward before descending in the extratropics (Butchart, 2014). In addition, synoptic disturbances in horizontal circulation play an important role in modulating O_3 variability in the UTLS region (Cooper et al., 1998;Gettelman et al., 2004;Jaeglé et al., 2017;Zhang et al., 2022). Several known circulation processes occur in the tropics, extratropics, and along the boundary between them (i.e., in the subtropics). In the tropics, tropical cyclones (especially the extreme form of typhoon) provide very favorable conditions for the entry of O_3-poor air from the surface to the lower stratosphere (i.e., TST) in the vicinity of the cyclone center and O_3-rich air from the lower stratosphere to the upper troposphere (i.e., STT) on the periphery of the cyclone (Zhan and Wang, 2012;Jiang et al., 2015;Das et al., 2016;Roux et al., 2020;Li et al., 2021). In the extratropics, STE is often related to upper-level frontal zone-jet-stream systems (Gettelman et al., 2011), in which the highly variable mid-latitude flow is largely affected by the north–south displacement of the westerly jet stream and eventually causes strong distortion of the tropopause through the redistribution of tropospheric and stratospheric air masses (i.e., tropopause fold). However, observations show that transport associated with episodic extratropical cyclones (particularly the extreme form of cut-off low, COL) is dominated by STT but also results in TST, which is sourced by warm conveyor-belt flows that bring lower troposphere air to the UTLS along isentropic surfaces (Jaeglé et al., 2017). In the subtropics, the most well-known STE process is Rossby wave breaking, which is a quasi-isentropic transport process across the sloped tropopause involving tropical upper troposphere air and extratropical lower stratosphere air (Holton et al., 1995). In addition, the Asia Summer Monsoon Anticyclone (ASMA) is well recognized as a prominent transport pathway for tropospheric pollutants to enter the stratosphere (Randel et al., 2010;Bian et al., 2020;Zhang et al., 2020). The ASMA is the largest dynamic system of the Northern Hemisphere during the boreal summer, consisting of convergent cyclonic flow in the lower troposphere and strong divergent anticyclonic flow in the UTLS. Controlled by the ASMA, thermal convection rapidly lofts lower troposphere air into the interior of the upper troposphere anticyclonic circulation, where it slowly ascends into the lower stratosphere. Overall, the strong variability of these multi-scale circulation processes in time and space shapes a highly variable distribution of O_3 in the UTLS region in different seasons and different geographical regions.

Northeast Asia, located between the middle and high latitudes, has a particularly complex and highly variable upper-level circulation regime throughout the year, which leads to a high degree of variability characteristic of the UTLS O_3 distribution. The dominant upper-level circulation system over this region is the East Asian Trough (EAT),

https://doi.org/10.5194/egusphere-2023-1393
Preprint. Discussion started: 24 October 2023

one of the strongest planetary-scale quasi-stationary troughs in the mid-latitudes, which further feeds a frequent occurrence of COLs (Nieto et al., 2005). COLs are defined as cold cyclonic systems that grow out of an upper-level trough, having become completely detached from the basic westerly current in the jet stream and subsequently lying equatorward of this westerly current. COLs are important synoptic systems associated with extratropical stratosphere-to-troposphere transport (Ancellet et al., 1994;Langford et al., 1996;Kuang et al., 2012;Yates et al., 2013;Li et al., 2015;Chen et al., 2022). Using 89 validated O_3 profiles, Song et al. (2016) investigated the influence of COLs on UTLS O_3 variability in Changchun, a city in Northeast China. Their results showed that, on average, COLs induced a 32% increase of O_3 in the UTLS region. Combining multiyear satellite and reanalysis data, Chen et al. (2019) performed another statistical investigation on the spatiotemporal change of UTLS O_3 induced by COLs over the Northeast Asia region. Their statistical results indicated that the magnitude and distribution of ozone enhancements were closely related to the evolution of COLs lifecycle. Different from the COLs, the ASMA has been considered to be an important contributor to troposphere-to-stratosphere transport over the Northeast Asia region via the shedding of secondary anticyclones (Honomichl and Pan, 2020;Fujiwara et al., 2021;Clemens et al., 2022;Peng et al., 2022). Two characteristic transport pathways were identified for shedding events: one characterized by eastward shedding in the troposphere, with subsequent slower northward transport into the stratosphere, and one characterized by poleward shedding into the stratosphere, with subsequent eastward advection to the downwind region (Ploeger et al., 2017;Clemens et al., 2022). O_3 evolution during transport in the shedding events shows a gradual change from monsoon anticyclone characteristics to lower stratospheric characteristics over ~1 week, indicating continuous mixing with the background atmosphere (Clemens et al., 2022). The studies cited above have demonstrated that upper-level circulation dynamics play an important role in redistributing O_3 in the UTLS region over the Northeast Asia region. However, most previous studies have been restricted to intensive events, certain circulation patterns, or patterns associated with ASMA only.

It is evident from previous studies that a comprehensive assessment of the co-variability of upper-level circulation patterns and UTLS O_3 distributions is needed for the Northeast Asia region in order to (a) fully grasp the coupling between STE and O_3 in the UTLS region and (b) improve the representation of such co-variability and coupling in the existing chemistry transport models as well as fully coupled Earth system models. Therefore, in the present study, we addressed the following questions:

1. Which typical upper-level circulation patterns prevail over the Northeast Asia region?
2. Is there a distinguishable signal in the UTLS O_3 distribution among different circulation patterns?
3. How do these different circulation patterns dynamically modulate the O_3 distribution in the UTLS region?

To answer the above-mentioned questions, we collect long-term observational data of multi-site ozonesondes and satellite-based remote sensing products to investigate UTLS O_3 variability over the Northeast Asia region in the framework of circulation pattern classification. By applying the self-organized mapping (SOM) technique to circulation data from reanalysis products, a twelve-class upper-level circulation pattern classification for the East Asia-Northwest Pacific region is constructed for the first time. The classification is then used to characterize the UTLS O_3 distribution over the Northeast Asia region, in both multi-site ozonesonde data and regional-scale satellite products. Finally, two normalized transport indicators—meridional transport indicator (*MTI*) and vertical transport indicator (*VTI*)—are developed to uncover the underlying transport mechanisms responsible for UTLS O_3 responses to different upper-level circulation patterns.

2 Data

2.1 Northeast Asia ozonesonde data

https://doi.org/10.5194/egusphere-2023-1393
Preprint. Discussion started: 24 October 2023

We collect ozonesonde data recorded at four Northeast Asia ozonesonde sites, namely, Beijing in China, Pohang in Korea, and Tateno and Sapporo in Japan (Table 1 and Fig. 1a), during a 21-year period from 2000 to 2020. These ozonesondes were performed by Carbon-Iodide (CI) and Electrochemical Concentration Cell (ECC) sensors (Table 1). In total, 3573 ozonesondes are available for this study: 903 from Beijing, 871 from Pohang, 988 from Tateno, and 811 from Sapporo. The dataset includes the regular weekly ozonesonde observation at ~14:00 local time (e.g., mostly every Tuesday at Beijing) and some short-term intensive measurements (particularly at Beijing and Tateno). The details of the ozonesonde sample distribution can be found in Fig. 1b. Similar to our previous study (Liao et al., 2021), data quality control is conducted for the ozonesonde measurements by identifying anomalous values and instrument malfunctioning via an inspection and selection procedure. The climatological O_3 vertical distributions are shown in Fig. 1c. In this study, we focus on the UTLS O_3 distribution. Considering that the average tropopause height is approximately 11 km above ground level (AGL) in the Northeast Asia region (Zhang et al., 2021), the UTLS is defined as the height range between 6 and 16 km AGL.

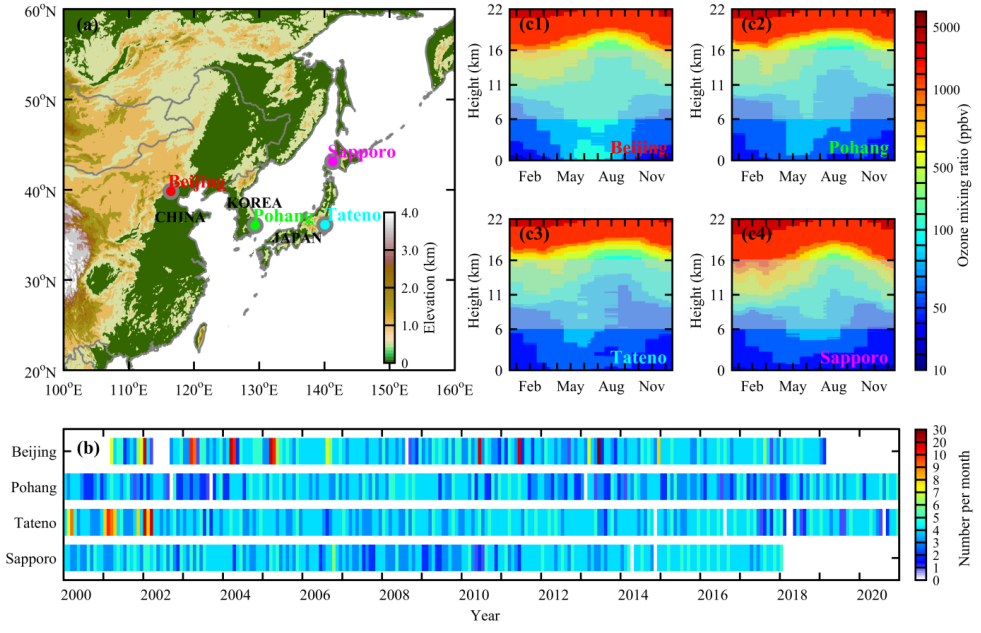

Figure 1. (a) Ozonesonde site distribution over the Northeast Asia region, (b) ozonesonde sample distribution by month from 2000 to 2020, (c) monthly median ozone (O_3) profile at: (1) Beijing, (2) Pohang, (3) Tateno, and (4) Sapporo. The marked height in (c) denotes the upper troposphere and lower stratosphere (UTLS) region.

Table 1. Information on the Northeast Asia ozonesondes used in this study

Site, Country	Longtitude/Latitude (deg)	Altitude (m)	Length of Record	Number of Profiles	Ozonesonde Sensors
Beijing, China	116.28/39.93	31.0	2001–2019	903	CI and ECC
Pohang, Korea	129.38/36.03	2.5	2000–2020	871	ECC
Tateno, Japan	140.10/36.10	31.0	2000–2020	988	CI and ECC
Sapporo, Japan	141.30/43.10	26.0	2000–2018	811	CI and ECC

2.2 Satellite-based observation data

The Atmospheric Infrared Sounder (AIRS) launched on NASA's Aqua satellite in May 2002 provides vertically resolved measurements of variable chemical species (Aumann et al., 2003). Several datasets of different

https://doi.org/10.5194/egusphere-2023-1393
Preprint. Discussion started: 24 October 2023

spatiotemporal resolutions are produced by the AIRS team. Here, we use level 3 version 6 data, including O_3 and CO, on a $1.0^o \times 1.0^o$ horizontal grid over the Northeast Asia region. Level 3 data are a quality-checked version of the level 2 swath products from AIRS, output on standard pressure levels. To maintain time consistency with the ozonesonde measurements, only AIRS data from the ascending stage (daytime, equatorial crossing time 13:30 local time) of the Aqua orbit are used in this study.

2.3 Atmospheric reanalysis data

ERA5 reanalysis data from the European Centre for Medium-Range Weather Forecasts (ECMWF) are applied to conduct upper-level circulation classification and investigate large-scale meteorological conditions. ERA5 is generated by 4-D variational (4DVAR) data assimilation of the ECMWF's Integrated Forecast System (IFS) and prediction from the CF41R2 model (Hersbach et al., 2020). The hourly ERA5 data have a 0.25 °×0.25 ° spatial resolution. In this study, we extract the ERA5 data at 06:00 UTC (approximately 14:00 local time in Northeast Asia) during 2000–2020 to maintain approximate time consistency with afternoon ozonesonde measurement. The domain of the extracted ERA5 data covers the East Asia-Northwest Pacific region (20 °N–60 °N and 105 °E–155 °E), with an approximate center located over the Northeast Asia region. The selected variables include geopotential height (GPH), potential vorticity (PV), and zonal wind at isobaric levels from 500 to 100 hPa.

3 Method

3.1 Self-organizing map circulation classification

Generalized upper-level circulation patterns over the East Asia-Northwest Pacific region (100^oE−160^oE, 20^oN−60^oN), obtained by applying the self-organizing map (SOM) clustering method, form the core of this study. The SOM method, developed by Kohonen (2001), can be characterized as a nonlinear mapping of high-dimensional input data onto a two-dimensional array of reference vectors (i.e., nodes or patterns). This method was originally developed for artificial neural networks but has been extensively applied in many fields of science, including the synoptic climatology (Hewitson and Crane, 2002). The size of a node array is often subjectively determined by the user, depending on the application. In general, fewer nodes will lead to a high level of generalization of the patterns but make the visualization and conceptualization of the results easier, whereas more nodes will increase the level of detail in regional features but reduce the statistical significance of the results owing to a decline in sample numbers assigned to each pattern. Compared with other traditional methods (e.g., PCA), an outstanding advantage of the SOM technique is that it treats synoptic categories as a continuum and presents both the basic and transitional patterns in an array on the SOM plane, which allows the classified patterns to be readily understood and visualized (Hewitson and Crane, 2002).

In this study, the SOM method is applied to 21 years (2000–2020) of daily ERA5 GPH data (7,671 samples). To better characterize upper-level circulation, GPH data for three layers—100, 250, and 500 hPa—are merged into a composite variable to conduct circulation classification. The 100, 250, and 500 hPa heights represent the lower stratosphere, tropopause layer, and upper troposphere, respectively. To ensure equal weighting for each layer, the gridded GPH data are normalized via z-score standardization layer by layer for each day using equation (1):

$$z_{i,j} = \frac{x_{i,j} - \mu}{\delta} \quad (1)$$

where $z_{i,j}$ is the standardized GPH at grid (i, j), $x_{i,j}$ represents the GPH at grid (i, j), μ denotes the regional mean of the GPH in the study domain (105^oE−155^oE, 20^oN−60^oN), and δ is the regional standard error of the GPH. Based on a subjective evaluation of variable matrix sizes of SOM nodes, a 3 × 4 array of nodes is finally selected to characterize upper-level circulation patterns. The 3 × 4 matrix size represents a compromise between adequately

https://doi.org/10.5194/egusphere-2023-1393
Preprint. Discussion started: 24 October 2023

resolved details of self-organized circulation patterns and statistically significant ozonesonde sample size assigned to each pattern (the minimum sample number is 20). Once the circulation patterns are determined, the meteorological and environmental variables for each day are assigned to one of the 12 patterns to perform further composite analysis. To avoid extreme influences, the composite analysis in this study is based on the median (as well as other percentiles) rather than the traditional mean.

3.2 Airflow backward trajectory calculation

The Hybrid Single-Particle Lagrangian Integrated Trajectory (HYSPLIT) model is a complete system for computing simple air parcel trajectories to complex dispersion and deposition simulations (Stein et al., 2015). This study uses the HYSPLIT model to calculate the airflow backward trajectories arriving at Beijing, Pohang, Tateno, and Sapporo. To achieve 21-year trajectory calculations, the National Centers for Environmental Prediction (NCEP) reanalysis data from 2000 to 2020 are adopted as input data to drive the HYSPLIT model. The 3-day (i.e., 72 h) backward trajectories are calculated at 14:00 local time per day for each ozonesonde site. The heights of the trajectory end-points are set at 8.0 and 14.0 km AGL, representing the upper troposphere and lower stratosphere, respectively.

3.3 Normalized airflow transport indicators

Since O_3 abundances in the stratosphere are far greater than those in the troposphere, cross-tropopause transport (i.e., STE) is thought to be primarily responsible for UTLS O_3 variability. Furthermore, since the tropopause height is usually sloped in the mid-latitude region, STE processes over this region can be driven by vertical motion and meridional transport.

We propose a normalized meridional transport indicator (*MTI*) based on the airflow backward trajectory to quantify the meridional transport. The *MTI* value is calculated as follows:

$$MTI = \frac{Lat_{mean}}{Lat_{end}} \quad (2)$$

where Lat_{mean} is the average latitude of the 3-day backward trajectory, and Lat_{end} is the latitude of the end-point (i.e., the latitude of the corresponding site). Values of *MTI* can be expected to vary around 1.0. If $MTI > 1.0$, air masses are controlled by southward transport from a higher latitude; if $MTI < 1.0$, air masses are controlled by northward transport from a lower latitude.

Given that trajectory error occurs in vertical motion, we track the vertical behaviors of satellite-based O_3 and CO to infer the direction (upward or downward) and magnitude of vertical motion. When air masses originate from a higher elevation (e.g., from the lower stratosphere or higher), they often contain more abundant O_3, but less CO. Conversely, if upper-level air masses originate from a lower elevation (e.g., from the surface layer), they usually contain more abundant CO, but less O_3. In previous studies, many scholars adopted ground-based observation of different chemical tracers to develop vertical transport indicators for identifying the stratospheric intrusion influence (Cristofanelli et al., 2009;Ma et al., 2014). Here, we transfer the ground-based tracer-to-tracer approach to satellite-based observations to diagnose bidirectional vertical transport processes in the UTLS region. We propose a normalized vertical transport indicator (*VTI*) to minimize the effects of seasonal variation. For a given day, a quantity *VTI*, which combines the AIRS-measured data of O_3 and CO, is determined as follows:

$$VTI = \frac{[O_3]}{[CO]} \quad (3)$$

where $[O_3]$ and [CO] denote the normalized O_3 and CO from their baseline climatology. For example, $[O_3]$ is a

https://doi.org/10.5194/egusphere-2023-1393
Preprint. Discussion started: 24 October 2023

daily O_3 concentration divided by its baseline climatology, and the baseline climatology is determined as the median of the 15-day (±7 days) moving O_3 concentration during the whole study period. Similar to the *MTI*, values of *VTI* can be expected to vary around 1.0. If *VTI* > 1.0, air masses are more likely controlled by downward transport from a higher elevation; if *VTI* < 1.0, air masses are controlled by upward transport from a lower elevation.

4 Results and discussion

4.1 Self-organized upper-level circulation patterns

Upper-level circulation over the East Asia-Northwest Pacific region is self-organized into 12 different circulation patterns by applying the SOM algorithm to daily standardized geopotential height at 100, 250, and 500 hPa from 2000–2020. Figure 2 shows the SOM plane featuring a 3 × 4 array of the self-organized circulation patterns (labeled as Node_1–12). Table 2 provides an overview of these circulation patterns and Figure 3 displays the monthly occurrence distribution of each circulation pattern. The SOM plane of Fig. 2 shows a reasonable topology property with the most dissimilar circulation patterns far away and the most similar patterns neighboring each other. The gradual transition between the neighboring circulation patterns reveals a subtle change in the positions and intensities of synoptic systems (roughs and ridges). There appear to be four basic patterns (i.e., Node_1, 4, 9, and 12) at the corner positions on the SOM plane and eight transitional patterns at central positions (Fig. 2). The frequency proportions of the four basic patterns are 13.2% (Node_1), 11.3% (Node_4), 10.8% (Node_9), and 13.5% (Node_12). The transitional patterns of Node_10 and Node_11 also contain a frequent occurrence (> 10%). In particular, Node_11 represents the most common pattern with a total occurrence frequency of up to 13.8%. In contrast, Node_7 is the most infrequent pattern, and its occurrence frequency is just 2.6% during the whole study period. Many of the patterns (e.g., Node_4, 1, and 8) prevail in only a few months. However, several patterns (e.g., Node_5–7) exhibit no distinct seasonality and are found throughout the year.

Table 2. Overview of the self-organized upper-level circulation patterns over the East Asia-Northwest Pacific region. The bolded fonts denote the four basic circulation patterns.

Pattern	Frequency (%)	Main synoptic systems
Node_1	13.2	Eastward-extended ASMA at 100 hPa and southeastward-retreated WPSH at 500 hPa
Node_2	5.4	Eastward-extended ASMA at 100 hPa and southward-retreated WPSH at 500 hPa
Node_3	4.5	Strong ASMA at 100 hPa and southward-retreated WPSH at 500 hPa
Node_4	11.3	Strong ASMA at 100 hPa and northwestward-extended WPSH at 500 hPa
Node_5	4.9	A shallow EAT with the trough line in the Siberia region
Node_6	5.4	A shallow EAT with the trough line in the Eastern Russia
Node_7	2.6	A shallow EAT with the trough line in the Sakhalin Island
Node_8	4.5	A shallow EAT with the trough line in the Northwest Pacific
Node_9	10.8	A broad and deep EAT with the trough line in the Siberia region
Node_10	10.0	A deep EAT with the trough line in the Eastern Russia
Node_11	13.8	A deep EAT with the trough line in the Sakhalin Island
Node_12	13.5	A broad and deep EAT with the trough line in the Northwest Pacific

https://doi.org/10.5194/egusphere-2023-1393
Preprint. Discussion started: 24 October 2023

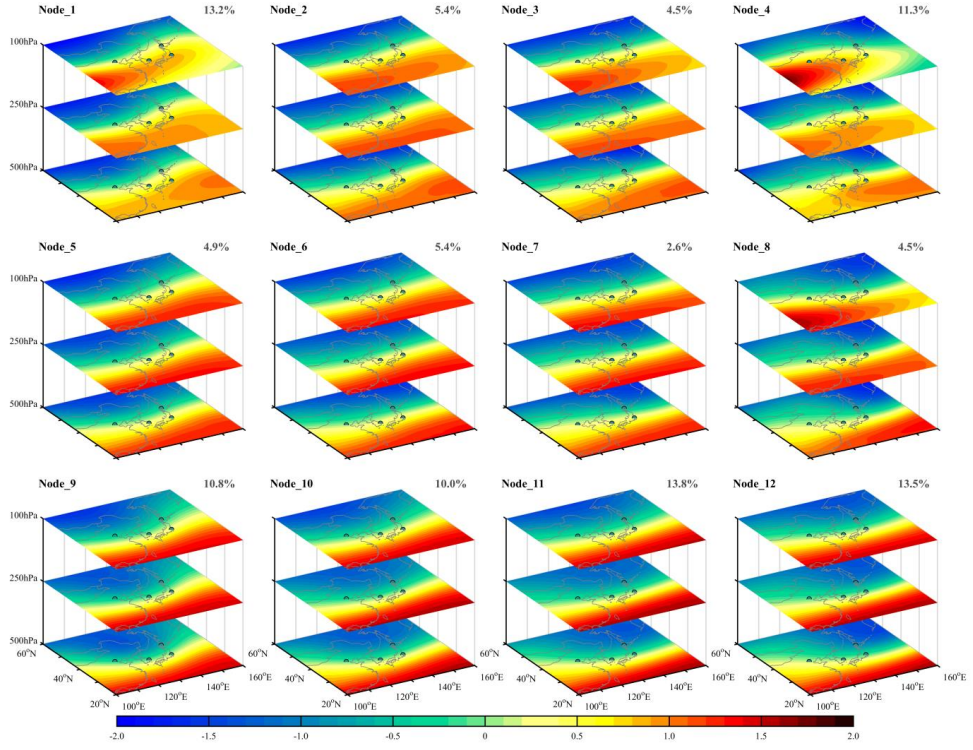

Figure 2. Self-organized upper-level circulation patterns (Node_1–12) over the East Asia-Northwest Pacific region. The shaded color denotes the normalized geopotential height with positive values representing high pressure. Dots represent the four ozonesonde sites (Beijing, Pohang, Tateno, and Sapporo) in the Northeast Asia region. Digits at the upper-right of each subplot denote the occurrence frequency of each circulation pattern.

In general, these different circulation patterns reflect the complex interactions among three well-known synoptic systems influencing the East Asia-Northwest Pacific region, including the ASMA, Western Pacific Subtropical High (WPSH), and EAT (Fig. 2). Node_1, which usually exists in mid-late spring, summer, and autumn, is controlled by eastward-extended ASMA at 100 hPa and southeastward-retreated WPSH at 500 hPa. The anomalous high pressure at 100 hPa over the Northwest Pacific region indicates the influence of eastward eddy shedding from the ASMA circulation, which is tied to the slightly southward development of EAT over the Siberia region. Node_4, the dominating circulation pattern during summertime, is characterized by strong ASMA at 100 hPa and northwestward-extended WPSH at 500 hPa. The ASMA-related thermal convection pushes the upper-level trough far away from the East Asian continent to present an anomalously eastern trough line in the Northwest Pacific. Node_9 is characterized by a broad and deep EAT with the trough line in the Siberia region (120°E). In this deep-trough pattern, a significant COL is formed in the upper troposphere over the Northeast China. The occurrence of Node_9 covers a period from October to June, with the most frequent occurrence in winter. Similar to Node_9, Node_12 is dominated by a broad and deep EAT, but the trough line position is located in the Northwest Pacific (150°E), further east than that in Node_9. The Node_12 pattern frequently occurs in mid-late winter, spring, and early summer. The other patterns contain transitional characteristics among the four basic patterns. Traversing patterns from bottom to top rows on the SOM plane presents a gradual weakening of the EAT accompanied by a

https://doi.org/10.5194/egusphere-2023-1393
Preprint. Discussion started: 24 October 2023

gradual strengthening of the ASMA and WPSH; traversing patterns from left to right columns show a gradual eastward movement of the EAT, reflecting synoptic-scale features of eastward propagating low-pressure systems on time scales of days.

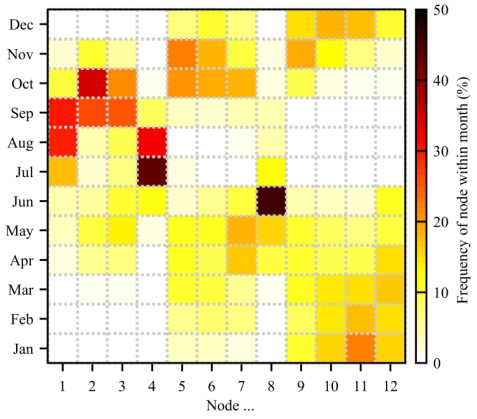

Figure 3. Monthly occurrence distribution of each circulation pattern

4.2. UTLS O_3 response to circulation patterns

Figure 4 shows the statistical percentile values (5%, 25%, 50%, 75%, 95% percentiles) of O_3 within two characteristic height ranges—upper troposphere (7.5–8.5 km) and lower stratosphere (13.5–14.5 km)—for days ascribed to each of the self-organized circulation patterns. The pattern-specific sample numbers are displayed in the right part of Fig. 4. The per-site sample number in each pattern is no less than 20, with the minimum belonging to Beijing in Node_7. The abundance of samples ensures that the percentile values have statistical significance. The upper-tropospheric O_3 generally presents the maximum median concentrations in Node_4 or Node_8, two typical summertime patterns. The maximum pattern-specific O_3 medians (25%–75% percentile interval) within 7.5–8.5 km height reach up to 109.1 (84.5–151.6) ppbv at Beijing in Node_4, 87.3 (71.1–107.8) ppbv at Pohang in Node_8, 81.2 (70.2–96.9) ppbv at Tateno in Node_8, and 87.6 (70.5–102.1) ppbv at Sapporo in Node_4. However, the lower-stratospheric median O_3 in these two patterns is moderate for Pohang, Tateno, and Sapporo and the lowest observed (157.1 ppbv) at Beijing in Node_4, among all circulation patterns. Affected by eastward eddy shedding of the ASMA, Node_1 is associated with the lowest lower-stratospheric median O_3 at Pohang (118.0 ppbv), Tateno (110.6 ppbv), and Sapporo (185.7 ppbv). By contrast, the lowest upper-tropospheric median O_3 concentrations are commonly associated with Node_5 (80.4 ppbv at Beijing) or Node_6 (61.7, 60.8, and 57.3 ppbv at Pohang, Tateno, and Sapporo, respectively). In these patterns at the bottom positions on the SOM plane (i.e., Node_9, 10, 11, and 12), the upper-tropospheric O_3 has a moderate concentration, whereas the lower-stratospheric O_3 reaches a much higher concentration. Depending on the site, the maximum lower-stratospheric median O_3 is distributed in different patterns. Specifically, the lower-stratospheric median O_3 at Pohang reaches its maximum of 361.7 ppbv in Node_10; the lower-stratospheric median O_3 at Tateno reaches its maximum of 334.8 ppbv in Node_10; the lower-stratospheric median O_3 concentrations at Beijing and Sapporo reach maxima (537.1 and 602.9 ppbv, respectively) in Node_11.

https://doi.org/10.5194/egusphere-2023-1393
Preprint. Discussion started: 24 October 2023

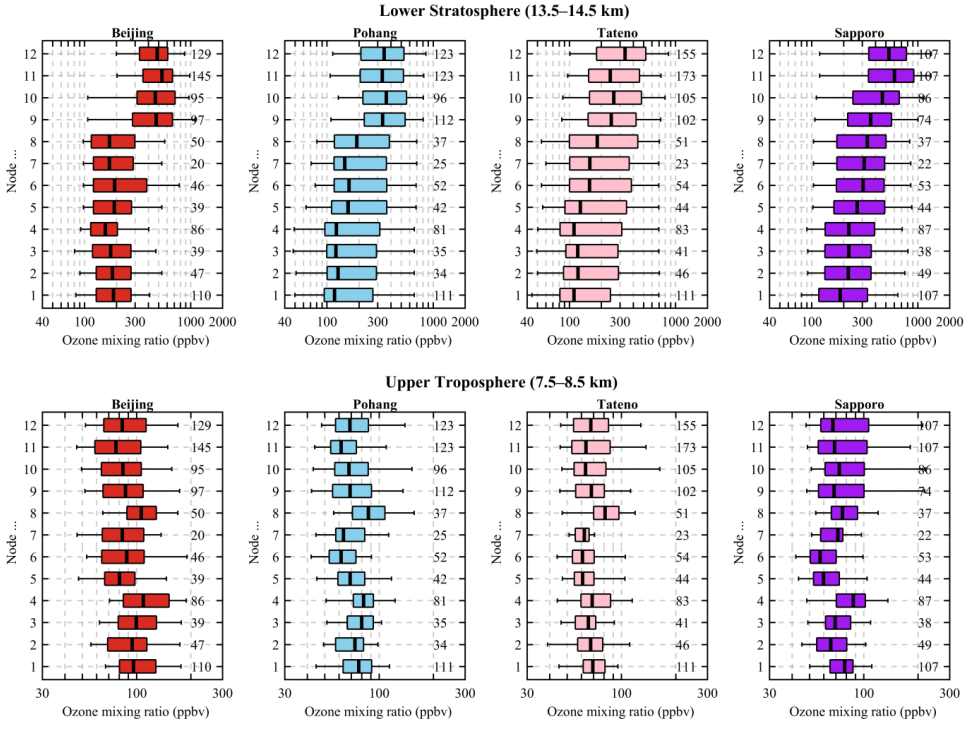

Figure 4. Ozone (O_3) mixing ratios within different altitude ranges (7.5–8.5 km representing the upper troposphere and 13.5–14.5 km representing the lower stratosphere) over Northeast Asia ozonesonde sites (Beijing, Pohang, Tateno, and Sapporo) under different upper-level circulation pattern conditions. Box-whisker plots denote the statistical values (5%, 25%, 50%, 75%, 95% percentiles) of O_3 mixing ratios. Digits to the right of each subplot denote the number of ozonesonde samples assigned to each of the circulation patterns.

We further composite the median O_3 profiles in the height range of 6.0–16.0 km corresponding to each circulation pattern for each ozonesonde site to investigate the modulation of upper-level circulation to UTLS O_3 vertical distribution over the Northeast Asia region (Fig. 5). Not surprisingly, subtle changes in upper-level circulation can propagate to the pattern-to-pattern variability in UTLS O_3 profiles. The O_3 profiles in the neighbor patterns exhibit a relatively small difference, whereas those in the corner patterns (Node_1, 4, 9, and 12) differ significantly. Traversing patterns from the top to bottom rows on the SOM plane, the inflections in the O_3 profiles are increasingly evident, and their occurrence heights become lower and lower, indicating a weakening influence of thermal convection. Owing to the seasonality of circulation patterns (Fig. 3), the pattern-specific median O_3 profiles inevitably contain substantial signals of seasonal O_3 variability. To eliminate the seasonal effect and highlight synoptic disturbances, the O_3 anomaly relative to baseline climatology is calculated. For a given day, the baseline climatology of the O_3 profiles is first generated by extracting the median O_3 layer-by-layer from a subset of ozonesondes in a 15-day (±7 days) moving window during the whole study period. The daily relative anomaly is then calculated by comparing the observations to climatology. Finally, the pattern-specific relative anomaly is composited according to different circulation patterns. The relative anomaly, rather than an absolute anomaly, adopted here allows for a better comparison among the different sites. As shown in Fig. 5, the cross-pattern O_3 anomaly changes in the lower stratosphere are more dramatic than the counterparts in the upper troposphere. The

https://doi.org/10.5194/egusphere-2023-1393
Preprint. Discussion started: 24 October 2023

upper-tropospheric O_3 anomalies are generally small (within ±10%); however, the lower-stratospheric O_3 anomalies change with patterns in a much wider range (−40% to 40%). These results suggest that the lower-stratospheric O_3 is more sensitive to synoptic-scale changes in upper-level circulation compared to the upper-tropospheric O_3.

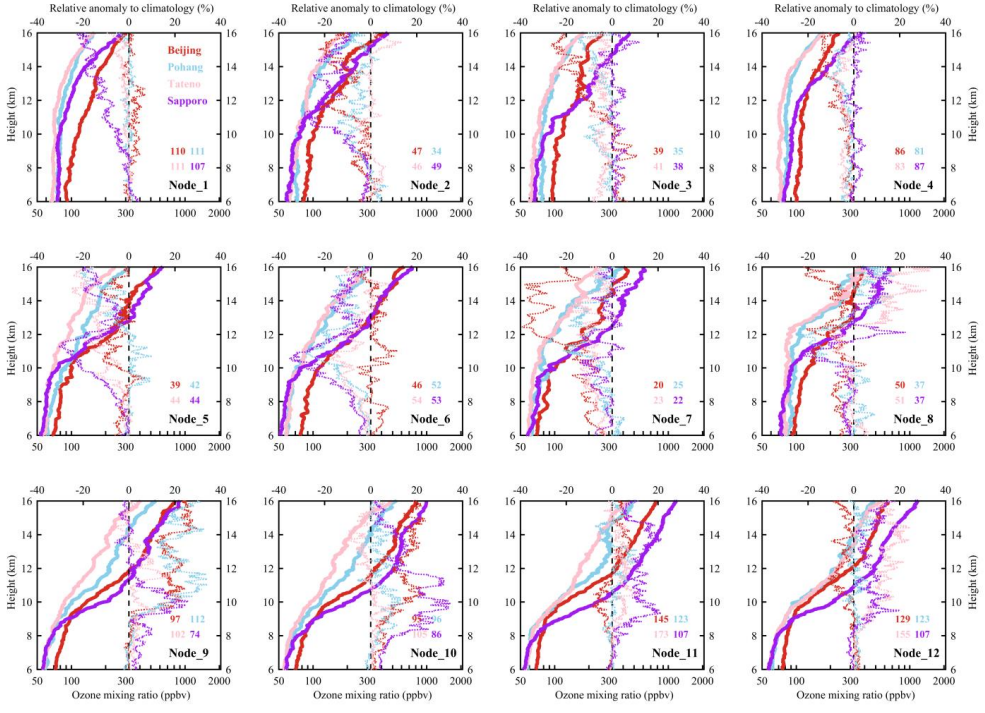

Figure 5. Sonde-based ozone (O_3) vertical distributions in the upper troposphere and lower stratosphere over Northeast Asia ozonesonde sites (Beijing, Pohang, Tateno, and Sapporo) under different upper-level circulation pattern conditions. Solid lines are the O_3 mixing ratios, and dashed lines denote the O_3 anomaly (%) relative to baseline climatology. Colorful digits are the numbers of ozonesonde samples belonging to each circulation pattern.

In each circulation pattern, the UTLS O_3 (anomaly) profiles differ largely at the different ozonesonde locations (Fig. 5). In the upper troposphere, the O_3 median at Beijing is always the highest among the four Northeast Asia ozonesonde sites. The highest upper-tropospheric O_3 at Beijing may be explained by the strongest photochemical production of tropospheric O_3 due to the highest emissions of O_3 precursors in China. In the lower stratosphere, the O_3 median at Sapporo is usually the highest among the four sites, except for in Node_1. The highest lower-stratospheric O_3 at Sapporo can be explained by the high latitude of Sapporo. The lower-stratospheric O_3 concentrations strongly depend on latitude among the four ozonesonde locations, following a high-to-low order from Sapporo to Beijing, Tateno, and Pohang. The latitude dependence is also well captured by space-based observations (Fig. 6 and Fig. 7). However, in Node_1, the lower-stratospheric O_3 at Beijing is significantly higher than at Sapporo. This phenomenon is not due to the explosive increase of lower-stratospheric O_3 at Beijing but is caused by the sudden decrease (negative anomaly) of lower-stratospheric O_3 at Sapporo. This decrease is likely the combined result of warm conveyor belt transport ahead of the upper-level trough and eastward eddy shedding from the ASMA circulation. Compared with the previous cross-pattern O_3 anomaly analysis, the within-pattern oddity in the multi-site O_3 concentration shown in Node_1 provides powerful evidence that upper-level circulation can

https://doi.org/10.5194/egusphere-2023-1393
Preprint. Discussion started: 24 October 2023

strongly modulate the lower-stratospheric O_3 distribution over short time scales.

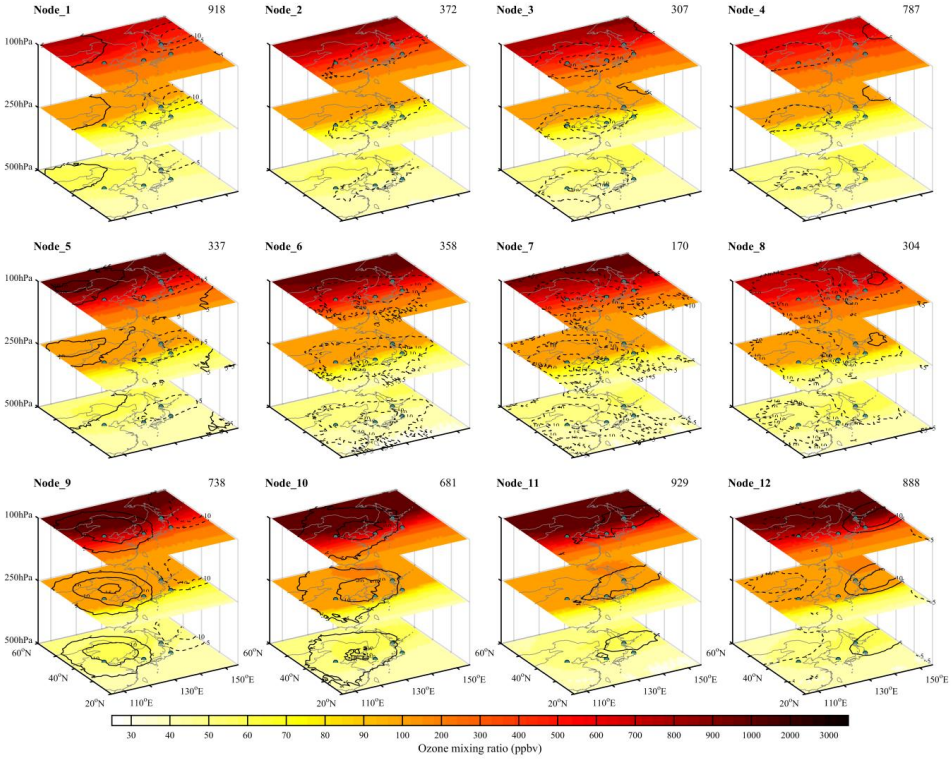

Figure 6. Satellite-based multilayer ozone (O_3; unit: ppbv) distributions over the East Asia-Northwest Pacific region under different upper-level circulation pattern conditions. Black solid (dashed) contours indicate positive (negative) anomalies (%) relative to baseline climatology with intervals of 5%. Dots denote the four ozonesonde sites (Beijing, Pohang, Tateno, and Sapporo) in the Northeast Asia region. The upper-right digits are the numbers of AIRS samples belonging to each circulation pattern.

The regional-scale co-variability of upper-level circulation patterns (Fig. 2) and space-based O_3 anomalies (Fig. 6) further confirms the synoptic modulation of UTLS O_3 distribution over the Northeast Asian region. As shown in Fig. 6, lower-stratospheric O_3 in all circulation patterns exhibits a similar spatial distribution with relatively higher concentrations in the high-latitude region and relatively lower concentrations in the low-latitude region, reflecting climatic-scale modulation of Brewer–Dobson circulation to the latitudinal O_3 gradient. By contrast, the spatial distribution of the O_3 anomaly reveals synoptic-scale modulation of upper-level horizontal circulation to UTLS O_3 variability. Using the sonde-based data set as a benchmark (Fig. 5), space-based O_3 anomalies are largely consistent with observations in the ozonesonde locations. From Fig. 6, the space-based O_3 anomaly distribution is highly sensitive to the upper-level circulation patterns, not only over the polluted mainland region but also over the Northwest Pacific region. The progression of the EAT appears critical in determining the location of elevated O_3 concentrations over the East Asia-Northwest Pacific region. Taking the bottom-row patterns as an example, the EAT moves eastwards with a trough line location from 120°E in Node_9 to 150°E in Node_12 (Fig. 2); accordingly, the positive O_3 anomaly zone transfers from the East Asia continent to the Northwest Pacific ocean (Fig. 6). Among

https://doi.org/10.5194/egusphere-2023-1393
Preprint. Discussion started: 24 October 2023

all circulation patterns, the highest O_3 anomalies are observed over Northeast China in Node_9. In this pattern, strong EAT accompanied by significant COL over the Northeast China region facilitates stratospheric O_3 intrusion, causing a noticeable enhancement in UTLS O_3 concentrations. In contrast, Node_7 displays the lowest O_3 anomaly among the 12 circulation patterns. In this pattern, the low O_3 anomaly zone nearly covers the whole East Asia continent, with the anomaly center near Beijing, coincident with the lowest sonde-based O_3 anomaly at this location (Fig. 5). However, as a transitional pattern, Node_7 has fewer defining circulation characteristics. The underlying mechanical understanding of the low O_3 anomaly in Node_7 requires additional investigation from a dynamic transport perspective.

4.3 Dynamic transport mechanism responsible for UTLS O_3 response

Figure 7 shows the composited meridional cross-sections of the O_3 mixing ratio, zonal wind speed, and dynamic tropopause height at 116.5°E (over Beijing), 129.5°E (over Pohang), and 140.5°E (approximately over Tateno and Sapporo) according to the different circulation patterns. The dynamic tropopause height is identified by two potential vorticity units (2-PVU). The zonal wind speed in Fig. 7 reveals the contrasting westerly jet stream across the different patterns, typically featuring a weak jet in the top-row patterns (Node_1, 2, 3, and 4) and a strong jet in the bottom-row patterns (Node_9, 10, 11, and 12). The maximum wind speed in the jet core is ~30 m s^{-1} in Node_1 and Node_4 but > 50 m s^{-1} in Node_9 and Node_12. Meanwhile, the jet core moves ~5 °latitude to the south from the top to bottom row patterns. However, the dynamic tropopause is always distorted in the vicinity of the northern edge of the westerly jet stream, particularly in the bottom patterns. The tropical tropopause differs little among all circulation patterns (~100 hPa), whereas the extratropical tropopause in the top-row patterns (200–250 hPa) is significantly higher than that in the bottom-row patterns (250–350 hPa). The tropopause is extremely sloped in the transitional area between the tropical and extratropical regions. This sloped tropopause is conducive to the occurrence of cross-tropopause transport because, near the sloped tropopause, the cross-tropopause transport can be aroused not only by vertical motion but also by meridional advection. Note that the four Northeast Asian ozonesonde sites are located exactly in the slope-tropopause area, implying that these sites are likely influenced by cross-tropopause transport. Deviations of pattern-specific tropopause from the baseline climatology are commonly larger in this sloped-tropopause area than at lower or higher latitudes, demonstrating a larger cross-tropopause transport influence over the Northeast Asia region. In the bottom-row patterns, the pattern-specific tropopause is generally lower than its baseline climatology, indicating a stratospheric intrusion influence. In the other patterns, the pattern-specific tropopause is commonly higher than its baseline climatology, indicating a tropospheric intrusion influence. At the site scale, different sites present different degrees of tropopause anomalies. Taking Node_1 as an example, the disparity between Sapporo and the other sites is evident in the tropopause anomaly, consistent with the differences in O_3 anomaly profile shape in Fig. 5. In Node_1, Sapporo corresponds to a significantly higher tropopause relative to its baseline climatology, indicating a strong tropospheric intrusion influence, which is evidently responsible for the large negative anomaly of lower-stratospheric O_3 over Sapporo, as shown in Fig. 5 and Fig. 6.

https://doi.org/10.5194/egusphere-2023-1393
Preprint. Discussion started: 24 October 2023

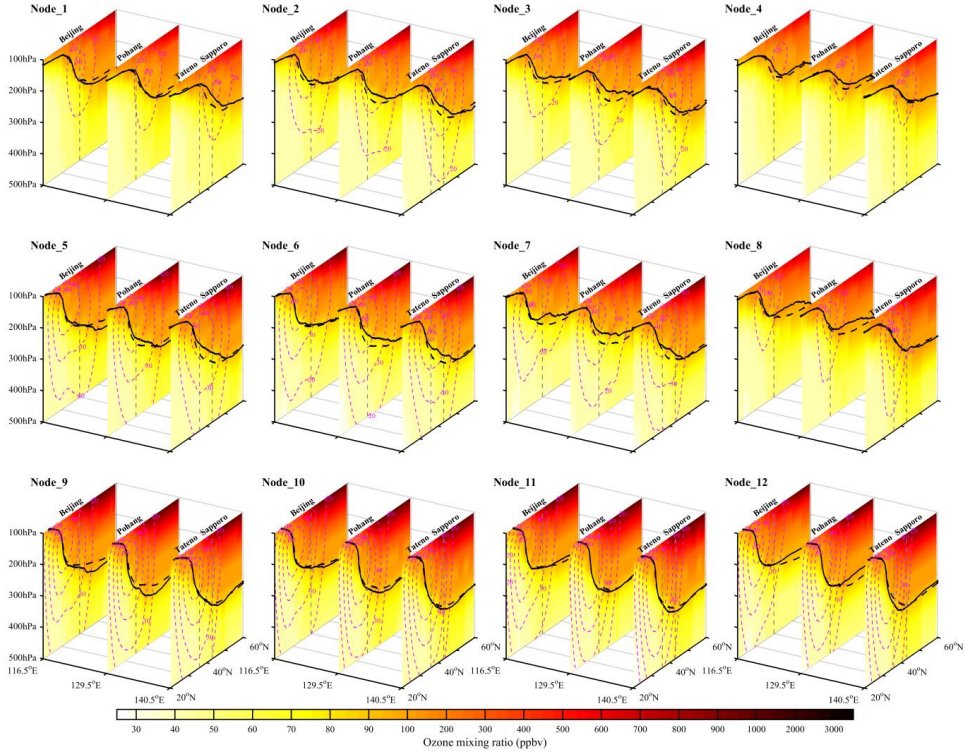

Figure 7. Pressure–latitude cross-sections of the ozone (O_3) mixing ratio, zonal wind speed (magenta dashed contours from 20 m s^{-1} with intervals of 10 m s^{-1}), and dynamic tropopause height (black lines) at 116.5°E (over Beijing), 129.5°E (over Pohang), and 140.5°E (approximately over Tateno and Sapporo) under different upper-level circulation pattern conditions. Black dashed lines denote pattern-specific baseline climatology of tropopause height. Grey dashed vertical lines point to the approximate locations of Beijing, Pohang, Tateno, and Sapporo.

Figure 8 shows the composited spatial distribution of the normalized vertical transport indicator (*VTI*) at 300 hPa (upper troposphere) and 150 hPa (lower stratosphere) according to the different circulation patterns. In conjunction with Fig. 2, it can be seen that large-scale vertical motion is strongly modulated by the position and intention of the prevailing upper-level trough (i.e., the EAT). Focusing on the East Asia-Northwest Pacific region, the downwelling zone (*VTI* > 1.05) is generally located southwest of the EAT and remains in step with the position variation of EAT across different patterns. Specifically, traversing patterns from the right to left columns shows an eastward shift of high *VTI* in response to the eastward propagating of EAT, whereas traversing patterns from the top to bottom row show increasing *VTI* in the downwelling zone as a response to the southward deepening of EAT. By contrast, the fore-trough area and areas far behind EAT are dominated by upwelling (*VTI* < 0.95). In the left-column patterns (Node_1, 5, and 9), Beijing is dominated by downdraft flow, and Sapporo is controlled by updraft motion. In the right-column patterns (Node_4, 8, and 12), Beijing is dominated by updraft flow, and Sapporo is controlled by downdraft motion. In these zones featuring significant vertical motion (*VTI* > 1.05 or *VTI* < 0.95), the *VTI* values at 300 hPa are always larger than those at 150 hPa, indicating stronger downdraft disturbance in the upper troposphere of the downwelling zone (VTI > 1.05), but stronger updraft disturbance in the lower stratosphere of the upwelling zone (*VTI* < 0.95). This phenomenon is particularly notable in the upwelling zone of the top-row patterns (Node_1,

https://doi.org/10.5194/egusphere-2023-1393
Preprint. Discussion started: 24 October 2023

2, 3, 4), reflecting an additive effect from ASMA-related deep convection. Previous studies have revealed that ASMA-related deep convection can effectively transport tropospheric tracers from the boundary layer into the UTLS region (Randel et al., 2010;Bian et al., 2020), resulting in relatively high mixing ratios of tropospheric tracers (such as CO) and relatively low mixing ratios of stratospheric tracers (such as O_3) within the anticyclone (Kumar et al., 2021;Babu et al., 2021;Peng et al., 2022). Since the normalized vertical transport indicator (i.e., *VTI*) filters out seasonal signals in chemical tracers, we cannot detect significantly low *VTI* values in the interior of anticyclonic circulation (i.e., ASMA). However, the synoptic signal of low *VTI* values is notably northeast of the anticyclone (e.g., East Mongolia and Northeast China) in Node_2, 3, and 4. This is likely due to the poleward shedding of the secondary anticyclone and the subsequent eastward advection to the downwind region. In Node_1, the eastward shedding of the ASMA allows for a greater impact of tropospheric invasion over the downstream regions (e.g., Korea and South Japan). With the aid of the warm conveyor belt in front of the EAT, the tropospheric tracers shedding from the ASMA can be further transported northward. This explains the significantly low *VTI* and O_3 values stretching from South Japan to Sakhalin Island in Node_1. Note that Node_7 is characterized by large-range strong upwelling motion (*VTI* < 1.0) over the East Asia continent. The upwelling center is very near Beijing, causing the largest negative O_3 anomaly in the lower stratosphere of Beijing (Fig. 5 and Fig. 6).

The composited backward trajectories terminating at 8 km (upper troposphere) and 14 km (lower stratosphere) over the Northeast Asia ozonesonde sites (Beijing, Pohang, Tateno, and Sapporo) according to upper-level circulation patterns are also illustrated in Fig. 8 to investigate the horizontal transport influences. For reference, the pattern-specific baseline climatology of the backward trajectory is further overlaid in Fig. 8. Besides, the *MTI* values (i.e., the normalized latitudinal transport indicator) are shown to the right of each subplot. Dominated by the westerly jet stream (Fig. 7), all composited trajectories in the different circulation patterns show air masses coming from western sources (Fig. 8). Even so, the transport pathway exhibits contrasting north-south fluctuation across different patterns. For brevity, we only provide a detailed description of the backward trajectory characteristics in the four basic patterns (i.e., Node_1, 4, 9, and 12). In Node_1, the backward trajectories terminating at Sapporo travel the low-latitude region (*MTI* ≤ 0.91), with a significant southward deviation compared with the climatological trajectory. In contrast, the backward trajectories arriving at Beijing exhibit a slightly high-altitude source (*MTI* ≥ 1.03). The lower-stratospheric trajectories in Node_4 are controlled by stable westerlies and have fewer fluctuations in latitude (1.01 ≤ *MTI* ≤ 1.04). However, the upper-tropospheric trajectories terminating at Pohang usually come from the low-latitude area (*MTI* = 0.95) along the northwest boundary of WPSH. In Node_9, these backward trajectories terminating at Beijing are dominated by high-latitude sources (*MTI* ≥ 1.13), while those arriving at Tateno pass over low-latitude sources (*MTI* ≤ 0.95). In contrast, the backward trajectories terminating at Sapporo experience zigzag transport, originating from high latitude, then turning to low latitude and finally turning northeastward towards Sapporo. Such a complex pathway is likely determined by the fore-trough position of Sapporo in this deep EAT pattern. For Node_12, all trajectories travel through high-latitude areas before moving to the ozonesonde sites (*MTI* ≥ 1.03), particularly these trajectories terminating at Sapporo (*MTI* ≥ 1.13). Overall, the position and intention of the prevailing EAT largely shape the cross-latitude transport pathway to the different ozonesonde sites among the different patterns. For example, traversing patterns from the top to bottom rows show a gradual increase in MTI values at almost all sites in response to the southward deepening of EAT; traversing patterns from the right to left columns show a gradual decrease of *MTI* values at Beijing, but increases at Tateno and Sapporo in response to the eastward propagating EAT. Previous studies showed that the low-pressure system is accompanied by enhanced meridional circulation that favors the southward invasion of air masses from high latitudes in the post-trough area (i.e., dry intrusion airstreams) and northward invasion of air masses from low latitudes in the fore-trough area (i.e., warm conveyor belt airstreams) (Chen et al., 2014;Jaegl éet al., 2017).

https://doi.org/10.5194/egusphere-2023-1393
Preprint. Discussion started: 24 October 2023

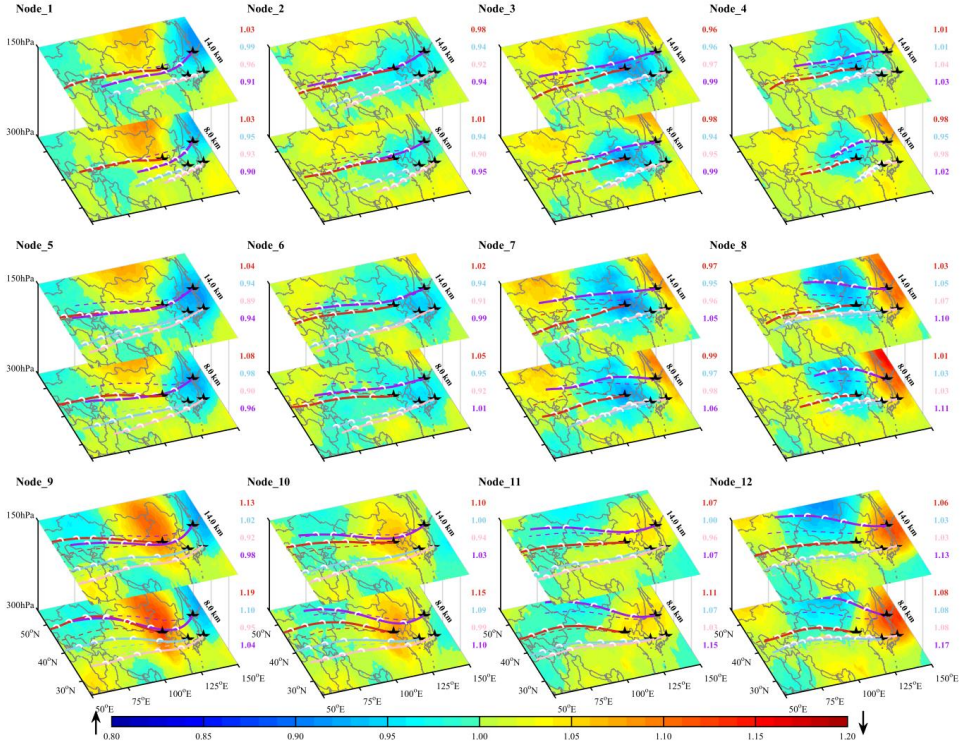

Figure 8. Backward trajectories (3-day) terminating at 8 km (upper troposphere) and 14 km (lower stratosphere) AGL over four Northeast Asia ozonesonde sites (Beijing, Pohang, Tateno, and Sapporo) corresponding to each upper-level circulation pattern. The solid lines with white circles indicate the pattern-specific composite of backward trajectories. The dashed lines denote the baseline climatology of the backward trajectory. Colored digits to the right of each subplot are the *MTI* values (i.e., the normalized meridional transport indicator) at each site and height. The background shows the spatial distribution of the *VTI* values (i.e., the normalized vertical transport indicator) at the adjacent layers to the terminating heights of the backward trajectory (i.e., 300 hPa corresponding to 8 km and 150 hPa corresponding to 14 km).

Based on findings from Fig. 4–Fig. 8, a quantitative relationship between the dynamic transport and UTLS O_3 is expected. Figure 9 presents the correlation coefficients (R) between the O_3 anomaly and transport indicator to examine how three-dimensional transport impacts UTLS O_3 over the Northeast Asia region. Here, the O_3 anomaly rather than the median O_3 is used so that all sites can be considered together. As shown in Fig. 9, lower-stratospheric (13.5–14.5 km) O_3 anomalies are significantly positively correlated with *MTI* at 14 km and *VTI* at 150 hPa. Considering all-site samples, the correlation coefficient between the lower-stratospheric O_3 anomaly and *MTI* at 14 km is 0.62, and between the lower-stratospheric O_3 anomaly and *VTI* at 150 hPa is 0.77. From the coefficient values, lower-stratospheric O_3 seems to have a stronger dependence on vertically downward transport than on meridionally southward transport. However, the higher correlation between the *MTI* and *VTI* (R = 0.79) suggests a co-occurrence property of vertical transport and meridional transport, implying that the relative importance of vertical motion and meridional transport to lower-stratospheric O_3 changes cannot be determined through simple correlation analysis, and requires further investigation based on numerous models. Correlation coefficients at

https://doi.org/10.5194/egusphere-2023-1393
Preprint. Discussion started: 24 October 2023

Beijing are commonly the highest (R > 0.90) among the four sites, indicating that the lower-stratospheric O_3 at Beijing is the most susceptible to upper-level circulation changes. This can be explained by the more westerly position of Beijing, located at the bottom–rear of the EAT, which receives more abundant O_3 from stratosphere intrusion. For the upper troposphere, the correlations between the O_3 anomaly and the transport indicator are weak (R < 0.40) and even statistically insignificant (e.g., at Beijing, Tateno, and Sapporo). These low correlations are within expectation because upper tropospheric O_3 is controlled not only by transport but also by photochemistry, which depends on a series of complex conditions, including photochemical-related meteorology, O_3 precursor concentration, and O_3 production sensitivity.

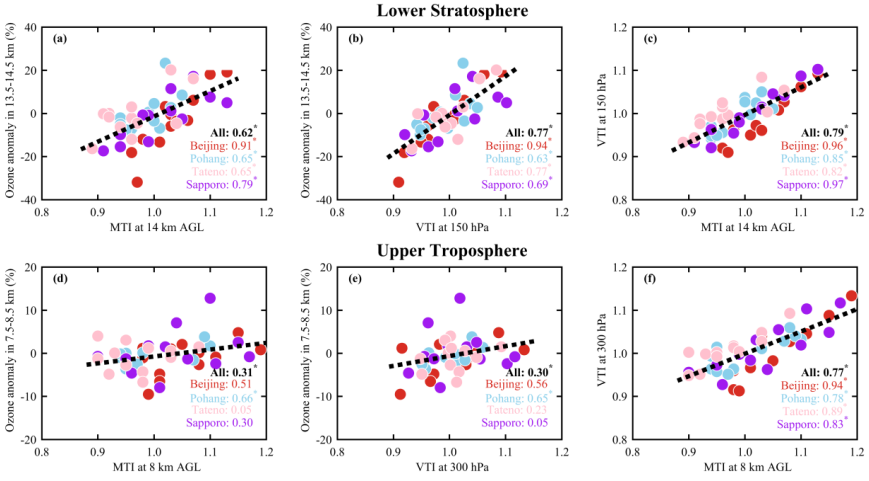

Figure 9. Scatterplots of within-pattern ozone (O_3) anomalies, the meridional transport indicator (*MTI*), and the vertical transport indicator (*VTI*) in the lower stratosphere (a–c) and upper troposphere (d–f). Correlation coefficients from all-site and single-site samples are shown by different-color digits. Dashed lines denote the least squares best-fit lines from all-site samples. The stars indicate a statistically significant correlation at a significance level of 0.05.

5 Conclusions

Large-scale circulation classification provides an ideal tool for understanding circulation dynamics and their association with local UTLS O_3 variability. In this study, daily upper-level circulation patterns are objectively characterized through the use of SOM and are further linked to the daily UTLS O_3 characteristics in the Northeast Asia region. A combination of sonde- and satellite-based datasets spanning 21 years (2000–2020) is used. Two novel transport indicators (i.e., meridional transport and vertical transport indicators) are developed to uncover the underlying transport mechanisms responsible for pattern-to-pattern UTLS O_3 responses. The following conclusions can be drawn from the analysis:

1. The 12 upper-level circulation patterns, allocated by SOM analysis based on daily GPH fields, represent different locations and intensities of troughs (cyclones) and ridges (anticyclones) in relation to each other and reflect the complex interactions among three well-acknowledged synoptic systems influencing the East Asia-Northwest Pacific region (i.e., ASMA, WPSH, and EAT).
2. All-altitude O_3 concentrations in the UTLS region show sensitivity to upper-level circulation patterns. The cross-pattern O_3 anomaly changes in the lower stratosphere (within ±40% deviation relative to baseline climatology) are more dramatic than counterparts in the upper troposphere (within ±10% deviation).

https://doi.org/10.5194/egusphere-2023-1393
Preprint. Discussion started: 24 October 2023

Moreover, the UTLS O_3 responses to circulation patterns differ significantly at different locations, depending on their relative positions to the predominant synoptic system.

3. The progression of the EAT appears critical in determining the location of elevated O_3 concentrations. Circulation patterns (Node_9, 10, 11, and 12) featuring the EAT show clear O_3 enhancement in the rear of the trough. With eastward propagation of the EAT, the O_3 enhancement zone moves eastwards from the East Asia continent to the Northwest Pacific. Conversely, the circulation pattern (Node_1) featuring the eastward shedding of the ASMA shows a decreased O_3 concentration, especially at Sapporo, and the negative O_3 anomaly zone stretches from South Japan to Sakhalin Island.
4. There are significant differences in transport dynamics among different circulation patterns, and the contrasting transport dynamics eventually determine the co-variability relationship between upper-level circulation and UTLS O_3 distribution. Positive O_3 anomalies are usually associated with post-trough downward and southward transport (i.e., stratosphere-to-troposphere transport), whereas negative O_3 anomalies are commonly associated with fore-trough upward and northward transport (i.e., troposphere-to-stratosphere transport). In the lower stratosphere, the correlation between O_3 anomalies and transport indicators ($R > 0.60$) is significantly stronger than that ($R < 0.40$) in the upper troposphere; the strongest correlation exists in the lower stratosphere of Beijing.

Overall, this work provides the first systematic assessment of observationally constrained UTLS O_3 variability associated with large-scale upper-level circulation patterns in the Northeast Asia region. The skill in characterizing the UTLS O_3 evolution shown by the circulation pattern classification indicates the potential for using it as a diagnostic/predictive tool for O_3 dynamics, which is a key component for the complete understanding and modeling of complex radiation–ozone-dynamic interactions controlling the atmospheric radiative budget in the UTLS region.

Data availability

Beijing's ozonesonde data are available from the first and second authors upon reasonable request (lzhiheng118@163.com and zjq@mail.iap.ac.cn), other datasets used for this paper are publicly accessible and can be found at the links below:
https://woudc.org/home.php?lang=en (Ozonesondes at Pohang, Tateno, and Sapporo);
https://disc.gsfc.nasa.gov/datasets?keywords=AIRS&page=1 (AIRS-based O_3 and CO data);
https://cds.climate.copernicus.eu/cdsapp#!/search?type=dataset (ERA5 Atmospheric reanalysis data);
http://www.arl.noaa.gov/ready/hysplit4.html (HYSPLIT model and input data);
http://www.cis.hut.fi/projects/somtoolbox/ (MATLAB SOM Toolbox).

Author contributions

ZL designed the study, carried out the analysis and wrote the first draft of the paper. JZ performed ozonesondes at Beijing and provided the related data. YP, XJ, PM, QW, ZC and LD participated in the discussions. JQ provided invaluable comments and revisions. All authors contributed to the writing and interpretation of the results.

Competing interests

The contact author has declared that neither they nor their co-authors have any competing interests.

Disclaimer

Publisher's note: Copernicus Publications remains neutral with regard to jurisdictional claims in published maps and institutional affiliations.

https://doi.org/10.5194/egusphere-2023-1393
Preprint. Discussion started: 24 October 2023

Acknowledgements

This work is supported by the Special Fund Project for Central-level Public Welfare Scientific Research Institutes (No. IUMKY2023), and the National Natural Science Foundation of China (Nos. 41975181 and 42293321).

Reference

Ancellet, G., Beekmann, M., and Papayannis, A.: Impact of a cutoff low development on downward transport of ozone in the troposphere, Journal of Geophysical Research: Atmospheres, 99, 3451-3468, https://doi.org/10.1029/93JD02551, 1994.

Attinger, R., Spreitzer, E., Boettcher, M., Forbes, R., Wernli, H., and Joos, H.: Quantifying the role of individual diabatic processes for the formation of PV anomalies in a North Pacific cyclone, Quarterly Journal of the Royal Meteorological Society, 145, 2454-2476, https://doi.org/10.1002/qj.3573, 2019.

Aumann, H. H., Chahine, M. T., Gautier, C., Goldberg, M. D., Kalnay, E., McMillin, L. M., Revercomb, H., Rosenkranz, P. W., Smith, W. L., Staelin, D. H., Strow, L. L., and Susskind, J.: AIRS/AMSU/HSB on the Aqua mission: design, science objectives, data products, and processing systems, IEEE Transactions on Geoscience and Remote Sensing, 41, 253-264, 10.1109/TGRS.2002.808356, 2003.

Babu, S. R., Ratnam, M. V., Basha, G., Pani, S. K., and Lin, N. H.: Structure, dynamics, and trace gas variability within the Asian summer monsoon anticyclone in the extreme El Nino of 2015-2016, Atmos Chem Phys, 21, 5533-5547, 10.5194/acp-21-5533-2021, 2021.

Bian, J. C., Li, D., Bai, Z. X., Li, Q., Lyu, D. R., and Zhou, X. J.: Transport of Asian surface pollutants to the global stratosphere from the Tibetan Plateau region during the Asian summer monsoon, Natl Sci Rev, 7, 516-533, 10.1093/nsr/nwaa005, 2020.

Butchart, N.: The Brewer-Dobson circulation, Rev Geophys, 52, 157-184, https://doi.org/10.1002/2013RG000448, 2014.

Chagnon, J. M., Gray, S. L., and Methven, J.: Diabatic processes modifying potential vorticity in a North Atlantic cyclone, Quarterly Journal of the Royal Meteorological Society, 139, 1270-1282, https://doi.org/10.1002/qj.2037, 2013.

Chen, D., Lü, D., and Chen, Z.: Simulation of the stratosphere-troposphere exchange process in a typical cold vortex over Northeast China, Science China Earth Sciences, 57, 1452-1463, 10.1007/s11430-014-4864-x, 2014.

Chen, D., Zhou, T. J., Ma, L. Y., Shi, C. H., Guo, D., and Chen, L.: Statistical Analysis of the Spatiotemporal Distribution of Ozone Induced by Cut-Off Lows in the Upper Troposphere and Lower Stratosphere over Northeast Asia, Atmosphere-Basel, 10, Artn 696
10.3390/Atmos10110696, 2019.

Chen, D., Zhou, T. J., Guo, D., and Ge, S. H.: Simulation of the Multi-Timescale Stratospheric Intrusion Processes in a Typical Cut-Off Low over Northeast Asia, Atmosphere-Basel, 13, Artn 68
10.3390/Atmos13010068, 2022.

Clemens, J., Ploeger, F., Konopka, P., Portmann, R., Sprenger, M., and Wernli, H.: Characterization of transport from the Asian summer monsoon anticyclone into the UTLS via shedding of low potential vorticity cutoffs, Atmos Chem Phys, 22, 3841-3860, 10.5194/acp-22-3841-2022, 2022.

Cooper, O. R., Moody, J. L., Davenport, J. C., Oltmans, S. J., Johnson, B. J., Chen, X., Shepson, P. B., and Merrill, J. T.: Influence of springtime weather systems on vertical ozone distributions over three North American sites, Journal of Geophysical Research: Atmospheres, 103, 22001-22013, https://doi.org/10.1029/98JD01801, 1998.

Cristofanelli, P., Calzolari, F., Bonafè, U., Duchi, R., Marinoni, A., Roccato, F., Tositti, L., and Bonasoni, P.: Stratospheric intrusion index (SI2) from baseline measurement data, Theoretical and Applied Climatology, 97, 317-325, 10.1007/s00704-008-0073-x, 2009.

Das, S. S., Ratnam, M. V., Uma, K. N., Subrahmanyam, K. V., Girach, I. A., Patra, A. K., Aneesh, S., Suneeth, K. V.,

https://doi.org/10.5194/egusphere-2023-1393
Preprint. Discussion started: 24 October 2023

Kumar, K. K., Kesarkar, A. P., Sijikumar, S., and Ramkumar, G.: Influence of tropical cyclones on tropospheric ozone: possible implications, Atmos. Chem. Phys., 16, 4837-4847, 10.5194/acp-16-4837-2016, 2016.

de F. Forster, P. M., and Shine, K. P.: Radiative forcing and temperature trends from stratospheric ozone changes, Journal of Geophysical Research: Atmospheres, 102, 10841-10855, https://doi.org/10.1029/96JD03510, 1997.

Fujiwara, M., Sakai, T., Nagai, T., Shiraishi, K., Inai, Y., Khaykin, S., Xi, H., Shibata, T., Shiotani, M., and Pan, L. L.: Lower-stratospheric aerosol measurements in eastward-shedding vortices over Japan from the Asian summer monsoon anticyclone during the summer of 2018, Atmos. Chem. Phys., 21, 3073-3090, 10.5194/acp-21-3073-2021, 2021.

Gettelman, A., Kinnison, D. E., Dunkerton, T. J., and Brasseur, G. P.: Impact of monsoon circulations on the upper troposphere and lower stratosphere, Journal of Geophysical Research: Atmospheres, 109, https://doi.org/10.1029/2004JD004878, 2004.

Gettelman, A., Hoor, P., Pan, L. L., Randel, W. J., Hegglin, M. I., and Birner, T.: The Extratropical Upper Troposphere And Lower Stratosphere, Rev Geophys, 49, Artn Rg3003 10.1029/2011rg000355, 2011.

Grams, C. M., Wernli, H., Böttcher, M., Čampa, J., Corsmeier, U., Jones, S. C., Keller, J. H., Lenz, C.-J., and Wiegand, L.: The key role of diabatic processes in modifying the upper-tropospheric wave guide: a North Atlantic case-study, Quarterly Journal of the Royal Meteorological Society, 137, 2174-2193, https://doi.org/10.1002/qj.891, 2011.

Hersbach, H., Bell, B., Berrisford, P., Hirahara, S., Horányi, A., Muñoz-Sabater, J., Nicolas, J., Peubey, C., Radu, R., Schepers, D., Simmons, A., Soci, C., Abdalla, S., Abellan, X., Balsamo, G., Bechtold, P., Biavati, G., Bidlot, J., Bonavita, M., De Chiara, G., Dahlgren, P., Dee, D., Diamantakis, M., Dragani, R., Flemming, J., Forbes, R., Fuentes, M., Geer, A., Haimberger, L., Healy, S., Hogan, R. J., Hólm, E., Janisková, M., Keeley, S., Laloyaux, P., Lopez, P., Lupu, C., Radnoti, G., de Rosnay, P., Rozum, I., Vamborg, F., Villaume, S., and Thépaut, J.-N.: The ERA5 global reanalysis, Quarterly Journal of the Royal Meteorological Society, 146, 1999-2049, https://doi.org/10.1002/qj.3803, 2020.

Hewitson, B. C., and Crane, R. G.: Self-organizing maps: applications to synoptic climatology, Climate Research, 22, 13-26, 2002.

Holton, J. R., Haynes, P. H., McIntyre, M. E., Douglass, A. R., Rood, R. B., and Pfister, L.: Stratosphere-troposphere exchange, Rev Geophys, 33, 403-439, https://doi.org/10.1029/95RG02097, 1995.

Honomichl, S. B., and Pan, L. L.: Transport From the Asian Summer Monsoon Anticyclone Over the Western Pacific, Journal of Geophysical Research: Atmospheres, 125, e2019JD032094, https://doi.org/10.1029/2019JD032094, 2020.

Jaeglé, L., Wood, R., and Wargan, K.: Multiyear Composite View of Ozone Enhancements and Stratosphere-to-Troposphere Transport in Dry Intrusions of Northern Hemisphere Extratropical Cyclones, Journal of Geophysical Research: Atmospheres, 122, 13,436-413,457, https://doi.org/10.1002/2017JD027656, 2017.

Jiang, Y. C., Zhao, T. L., Liu, J., Xu, X. D., Tan, C. H., Cheng, X. H., Bi, X. Y., Gan, J. B., You, J. F., and Zhao, S. Z.: Why does surface ozone peak before a typhoon landing in southeast China?, Atmos. Chem. Phys., 15, 13331-13338, 10.5194/acp-15-13331-2015, 2015.

Kohonen, T.: Self-organizing maps, 3rd edn. Springer, London, 2001.

Kuang, S., Newchurch, M. J., Burris, J., Wang, L., Knupp, K., and Huang, G.: Stratosphere-to-troposphere transport revealed by ground-based lidar and ozonesonde at a midlatitude site, Journal of Geophysical Research: Atmospheres, 117, https://doi.org/10.1029/2012JD017695, 2012.

Kumar, K. R., Singh, B. B., and Kumar, K. N.: Intriguing aspects of Asian Summer Monsoon Anticyclone Ozone variability from Microwave Limb Sounder measurements, Atmospheric Research, 253, 105479, https://doi.org/10.1016/j.atmosres.2021.105479, 2021.

Lacis, A. A., Wuebbles, D. J., and Logan, J. A.: Radiative forcing of climate by changes in the vertical distribution of ozone, Journal of Geophysical Research: Atmospheres, 95, 9971-9981, https://doi.org/10.1029/JD095iD07p09971, 1990.

Langford, A. O., Masters, C. D., Proffitt, M. H., Hsie, E. Y., and Tuck, A. F.: Ozone measurements in a tropopause fold

https://doi.org/10.5194/egusphere-2023-1393
Preprint. Discussion started: 24 October 2023

associated with a cut-off low system, Geophysical Research Letters, 23, 2501-2504, https://doi.org/10.1029/96GL02227, 1996.

Li, D., Bian, J., and Fan, Q.: A deep stratospheric intrusion associated with an intense cut-off low event over East Asia, Science China Earth Sciences, 58, 116-128, 10.1007/s11430-014-4977-2, 2015.

Li, D., Vogel, B., Müller, R., Bian, J., Günther, G., and Riese, M.: Tropical Cyclones Reduce Ozone in the Tropopause Region Over the Western Pacific: An Analysis of 18 Years Ozonesonde Profiles, Earth's Future, 9, e2020EF001635, https://doi.org/10.1029/2020EF001635, 2021.

Liao, Z. H., Ling, Z. H., Gao, M., Sun, J. R., Zhao, W., Ma, P. K., Quan, J. N., and Fan, S. J.: Tropospheric Ozone Variability Over Hong Kong Based on Recent 20 years (2000-2019) Ozonesonde Observation, J Geophys Res-Atmos, 126, ARTN e2020JD033054
10.1029/2020JD033054, 2021.

Ma, J., Lin, W. L., Zheng, X. D., Xu, X. B., Li, Z., and Yang, L. L.: Influence of air mass downward transport on the variability of surface ozone at Xianggelila Regional Atmosphere Background Station, southwest China, Atmos Chem Phys, 14, 5311-5325, 10.5194/acp-14-5311-2014, 2014.

Martius, O., Schwierz, C., and Davies, H. C.: Tropopause-Level Waveguides, Journal of the Atmospheric Sciences, 67, 866-879, https://doi.org/10.1175/2009JAS2995.1, 2010.

Monks, P. S., Archibald, A. T., Colette, A., Cooper, O., Coyle, M., Derwent, R., Fowler, D., Granier, C., Law, K. S., Mills, G. E., Stevenson, D. S., Tarasova, O., Thouret, V., von Schneidemesser, E., Sommariva, R., Wild, O., and Williams, M. L.: Tropospheric ozone and its precursors from the urban to the global scale from air quality to short-lived climate forcer, Atmos Chem Phys, 15, 8889-8973, 10.5194/acp-15-8889-2015, 2015.

Nieto, R., Gimeno, L., De La Torre, L., Ribera, P., Gallego, D., Garcia-Herrera, R., Garcia, J. A., Nunez, M., Redano, A., and Lorente, J.: Climatological features of cutoff low systems in the Northern Hemisphere, J Climate, 18, 3085-3103, Doi 10.1175/Jcli3386.1, 2005.

Olsen, M. A., Schoeberl, M. R., and Douglass, A. R.: Stratosphere-troposphere exchange of mass and ozone, Journal of Geophysical Research: Atmospheres, 109, https://doi.org/10.1029/2004JD005186, 2004.

Peng, K., Luo, J., Mu, J., Cao, X., Tian, H., Shang, L., and Guo, Y.: Impact of intensity variability of the Asian summer monsoon anticyclone on the chemical distribution in the upper troposphere and lower stratosphere, Atmospheric and Oceanic Science Letters, 15, 100144, https://doi.org/10.1016/j.aosl.2021.100144, 2022.

Peters, D. H. W., Schneidereit, A., Bügelmayer, M., Zülicke, C., and Kirchner, I.: Atmospheric Circulation Changes in Response to an Observed Stratospheric Zonal Ozone Anomaly, Atmosphere-Ocean, 53, 74-88, 10.1080/07055900.2013.878833, 2015.

Petzoldt, K., Naujokat, B., and Neugebohren, K.: Correlation between stratospheric temperature, total ozone, and tropospheric weather systems, Geophysical Research Letters, 21, 1203-1206, https://doi.org/10.1029/93GL03020, 1994.

Ploeger, F., Konopka, P., Walker, K., and Riese, M.: Quantifying pollution transport from the Asian monsoon anticyclone into the lower stratosphere, Atmos Chem Phys, 17, 7055-7066, 10.5194/acp-17-7055-2017, 2017.

Randel, W. J., Park, M., Emmons, L., Kinnison, D., Bernath, P., Walker, K. A., Boone, C., and Pumphrey, H.: Asian Monsoon Transport of Pollution to the Stratosphere, Science, 328, 611-613, 10.1126/science.1182274, 2010.

Riese, M., Ploeger, F., Rap, A., Vogel, B., Konopka, P., Dameris, M., and Forster, P.: Impact of uncertainties in atmospheric mixing on simulated UTLS composition and related radiative effects, J Geophys Res-Atmos, 117, Artn D16305
10.1029/2012jd017751, 2012.

Roux, F., Clark, H., Wang, K. Y., Rohs, S., Sauvage, B., and Nédélec, P.: The influence of typhoons on atmospheric composition deduced from IAGOS measurements over Taipei, Atmos. Chem. Phys., 20, 3945-3963, 10.5194/acp-20-3945-2020, 2020.

https://doi.org/10.5194/egusphere-2023-1393
Preprint. Discussion started: 24 October 2023

Song, Y. S., Lu, D. R., Li, Q., Bian, J. C., Wu, X., and Li, D.: The impact of cut-off lows on ozone in the upper troposphere and lower stratosphere over Changchun from ozonesonde observations, Adv Atmos Sci, 33, 135-150, 10.1007/s00376-015-5054-2, 2016.

Stein, A. F., Draxler, R. R., Rolph, G. D., Stunder, B. J. B., Cohen, M. D., and Ngan, F.: NOAA's HYSPLIT Atmospheric Transport and Dispersion Modeling System, Bulletin of the American Meteorological Society, 96, 2059-2077, 10.1175/BAMS-D-14-00110.1, 2015.

Yates, E. L., Iraci, L. T., Roby, M. C., Pierce, R. B., Johnson, M. S., Reddy, P. J., Tadic, J. M., Loewenstein, M., and Gore, W.: Airborne observations and modeling of springtime stratosphere-to-troposphere transport over California, Atmos Chem Phys, 13, 12481-12494, 10.5194/acp-13-12481-2013, 2013.

Zhan, R., and Wang, Y.: Contribution of tropical cyclones to stratosphere-troposphere exchange over the northwest Pacific: Estimation based on AIRS satellite retrievals and ERA-Interim data, Journal of Geophysical Research: Atmospheres, 117, https://doi.org/10.1029/2012JD017494, 2012.

Zhang, J., Wu, X., Bian, J., Xia, X., Bai, Z., Liu, Y., Cai, Z., Huo, J., and Lyu, D.: Aerosol variations in the upper troposphere and lower stratosphere over the Tibetan Plateau, Environ Res Lett, 15, 094068, 10.1088/1748-9326/ab9b43, 2020.

Zhang, J. Q., Li, D., Bian, J. C., Xuan, Y. J., Chen, H. B., Bai, Z. X., Wan, X. W., Zheng, X. D., Xia, X. G., and Lu, D. R.: Long-term ozone variability in the vertical structure and integrated column over the North China Plain: results based on ozonesonde and Dobson measurements during 2001-2019, Environ Res Lett, 16, Artn 074053 10.1088/1748-9326/Ac109f, 2021.

Zhang, Y., Li, J., Yang, W., Du, H., Tang, X., Ye, Q., Wang, Z., Sun, Y., Pan, X., Zhu, L., and Wang, Z.: Influences of stratospheric intrusions to high summer surface ozone over a heavily industrialized region in northern China, Environ Res Lett, 17, 094023, 10.1088/1748-9326/ac8b24, 2022.